Heliyon 9 (2023) e13583

Contents lists available at ScienceDirect

Heliyon

journal homepage: www.cell.com/heliyon

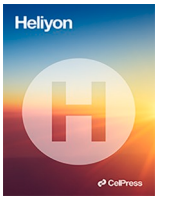

Research article

Extremely reduced loss tangent with retaining ultra high dielectric permittivity in Mg^{2+}-doped $La_{1.9}Sr_{0.1}NiO_4$ ceramics

Keerati Meeporn [a], Narong Chanlek [b], Pornjuk Srepusharawoot [c], Prasit Thongbai [c,*]

[a] Materials Science and Nanotechnology Program, Faculty of Science, Khon Kaen University, Khon Kaen 40002, Thailand
[b] Synchrotron Light Research Institute (Public Organization), 111 University Avenue, Muang District, Nakhon Ratchasima 30000, Thailand
[c] Giant Dielectric and Computational Design Research Group (GD-CDR), Department of Physics, Institute of Nanomaterials Research and Innovation for Energy (IN–RIE), Faculty of Science, Khon Kaen University, Khon Kaen 40002, Thailand

ARTICLE INFO

Keywords:
Nickelate
Giant dielectric properties
Loss tangent
DC conduction
Maxwell–Wagner polarization

ABSTRACT

An extremely reduced loss tangent while retaining ultrahigh dielectric permittivity can be successfully obtained in $La_{1.9}Sr_{0.1}NiO_4$ ceramics by doping with Mg^{2+} ions. A single phase of $La_{1.9}Sr_{0.1}NiO_4$ was detected in all the sintered ceramics, while the lattice parameters increased with increasing doping concentration, indicating that Mg^{2+} ions can enter the Ni^{2+} sites. A highly dense microstructure is achieved. Microstructural analysis revealed that Mg^{2+} ions disperse well in the microstructure of $La_{1.9}Sr_{0.1}NiO_4$ ceramics. Interestingly, ultra–high dielectric permittivity of approximately 8.11×10^5 at 1 kHz is achieved in the $La_{1.9}Sr_{0.1}Ni_{0.6}Mg_{0.4}O_4$ ceramic, while the loss tangent is significantly reduced by two orders of magnitude compared to the undoped $La_{1.9}Sr_{0.1}NiO_4$ ceramic. The DC conductivity significantly decreased by three orders of magnitude. The giant dielectric responses are described by Maxwell–Wagner polarization and small polaron hopping mechanisms. Thus, the significant reduction in the loss tangent can be attributed to the significantly enhanced resistance of the grain boundaries.

1. Introduction

Giant dielectric permittivity materials such as $CaCu_3Ti_4O_{12}$ (CCTO) and isostructural $ACu_3Ti_4O_{12}$-oxides [1–10], CuO [11], co-doped NiO-based oxides [12,13], $AFe_{1/2}B_{1/2}O_3$ (A = Ca, Sr, Ba; B = Sb, Ta, Nb) [14], co-doped TiO_2-based oxides [15–22], co-doped $SrTiO_3$-based oxides [23], and $Ln_{2-x}Sr_xNiO_4$ (*Ln* = La, Nd, and Sm) (*Ln*SNO) ceramics [24–30], have been widely investigated in recent years. These giant dielectric materials (or colossal-permittivity materials) can exhibit extreme values of dielectric permittivity (ε') of approximately 10^4–10^6 compared to those of ferroelectric materials (*e.g.*, $BaTiO_3$-based oxides), which are currently used in multilayer ceramic capacitors (MLCCs). In addition to MLCCs, these newly discovered giant dielectric materials have high potential for use in high-energy-density storage devices when some important material parameters can be improved [31].

*Ln*SNO is a promising giant dielectric oxide. *Ln*SNO ceramics exhibited extremely large $\varepsilon' \approx 10^5$–$10^6$ in the radio frequency range, while a high $\varepsilon' \approx 10^4$ was retained in the GHz region [25]. By considering the aspects of materials science coupled with resource strategies and resource management, *Ln*SNO has been judged to be potentially critical in the future compared to CCTO and $BaTiO_3$ ceramics [32]. Unfortunately, the great questions on which practical applications of *Ln*SNO ceramics can be developed remain. First, the low–frequency loss tangent of all *Ln*SNO ceramics is generally very large ($\tan\delta \approx 10^2$–10^3) among all giant dielectric–permittivity

* Corresponding author.
E-mail address: pthongbai@kku.ac.th (P. Thongbai).

https://doi.org/10.1016/j.heliyon.2023.e13583
Received 12 December 2022; Received in revised form 3 February 2023; Accepted 3 February 2023
Available online 9 February 2023

materials [25–28,33]. Second, besides the N_2−annealed $Nd_2NiO_{4+\delta}$ ceramic [34], ε' the values in all frequency ranges were strongly dependent on temperature, especially in the high-temperature range [35–38].

The giant dielectric response (GDR) in *Ln*SNO has been explained to be the extrinsic or intrinsic effect, that is, the sample–electrode effect [39] or small polaronic hopping mechanism [25,33,38,40]. Most recently, we have clearly shown that the GDR in $La_{1.7}Sr_{0.3}NiO_4$ results from a combination of the non-Ohmic contact between the sample−electrode interface and small polaronic hopping effects [24]. The GDRs resulting from these two effects are usually accompanied by a large DC conductivity, and hence, the tanδ value [41]. We have experimentally demonstrated that the dominant electrode effect in $La_{1.7}Sr_{0.3}NiO_4$ ceramics can be significantly reduced (or perhaps concealed) by enhancing the grain boundary resistance, which can be achieved by doping with Mg^{2+} ions with Ni^{2+} sites [24]. This experimental result was consistent with the theoretical prediction proposed by Li et al. [42]. As a result, the DC conductivity and tanδ of the $La_{1.7}Sr_{0.3}NiO_4$ ceramics decreased significantly. Furthermore, a significantly reduced tanδ with excellent temperature stability of ε' (at 1 MHz) in the temperature range of 250–450 K was obtained in $La_{1.5}Sr_{0.5}NiO_4$ (LSNO)–$xSiO_2$ composites, which was attributed to the formation of insulating grain boundaries [28]. Thus, it is reasonable to expect that the greatly enhanced resistance of the grain boundary can improve the dielectric properties of giant dielectric oxides [6,15,24,43–45]. Unfortunately, in both cases, the DC conductivities and related tanδ values for the $La_{1.5}Sr_{0.5}NiO_4$–$0.8SiO_2$ and Mg^{2+}−doped $La_{1.7}Sr_{0.3}NiO_4$ ceramics were still too large. This may be due to the large number of Sr^{2+} ions, which can induce Ni^{2+} to Ni^{3+} ions due to charge compensation. The polaronic concentration is directly dependent on the Sr^{2+} content.

Therefore, the aim of this work is to provide a new route to simultaneously reduce the low-frequency tanδ value of $La_{1.9}Sr_{0.1}NiO_4$ ceramics and improve the temperature stability ε' without any significant effect on very large ε' values ($\approx 8.1 \times 10^5$ at 1 kHz). Enhancement of the insulating grain boundary resistivity is the primary cause of the decrease in tanδ of $La_{1.9}Sr_{0.1}NiO_4$ ceramics by doping with Mg^{2+} ions. A new strategy for the improvement of the temperature dependence of ε' is also proposed by means of an enlarged polaronic size by reducing the Sr^{2+} content ($x = 0.1$ for $La_{2-x}Sr_xNiO_4$) to shorten the long–range motion of free charge carriers (holes) and/or confining them inside an individual grain.

2. Experimental details

$La_{1.9}Sr_{0.1}Ni_{1-x}Mg_xO_4$ ($x = 0$, 0.3, 0.4, and 0.5) materials were prepared using a chemical combustion route and sintered at 1375 °C for 6 h in air. The details of the chemical combustion method for preparing $La_{1.9}Sr_{0.1}Ni_{1-x}Mg_xO_4$ materials are provided elsewhere [24,29]. The sintered $La_{19}Sr_{01}NiO_4$, $La_{19}Sr_{01}Ni_{0.7}Mg_{0.3}O_4$, $La_{19}Sr_{01}Ni_{0.6}Mg_{0.4}O_4$, and $La_{19}Sr_{01}Ni_{0.5}Mg_{0.5}O_4$ were abbreviated as the LSNO, LSNO_Mg03, LSNO_Mg04, and LSNO_Mg05 ceramics, respectively.

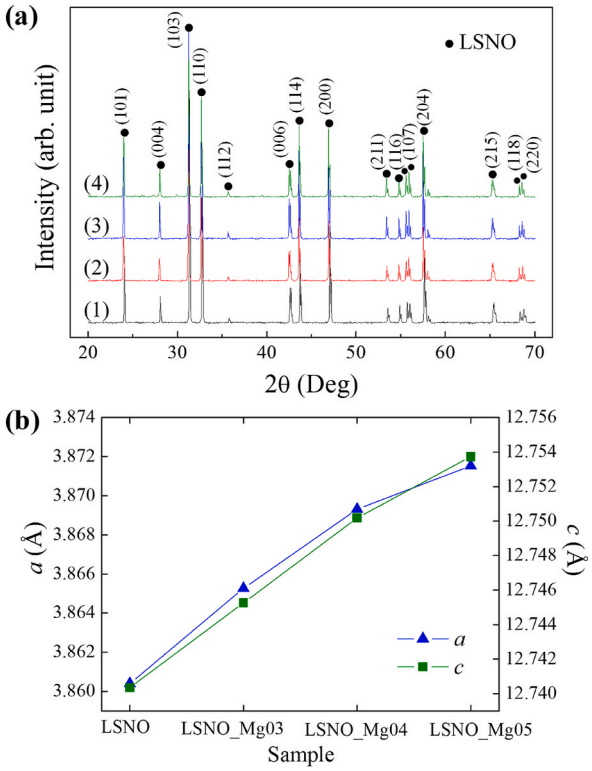

Fig. 1. (a) XRD patterns of (1) LSNO, (2) LSNO_Mg03, (3) LSNO_Mg04, and (4) LSNO_Mg05. (b) Lattice parameters (a and c) of all the sintered ceramics.

The prepared ceramic samples were characterized by scanning electron microscopy (SEM) (LEO 1450VP, UK). For SEM observation, the surface of the as-sintered samples was polished and thermally etched at 1100 °C for 0.5 h. The density was measured using the Archimedes' method. The presence of each type of ion in the $La_{1.9}Sr_{0.1}Ni_{1-x}Mg_xO$ ceramics was confirmed by energy-dispersive X-ray spectroscopy (EDS, HITACHI SU8030, Japan). The structure and phase composition were confirmed using X-ray diffraction (XRD) spectroscopy (PANalytical, EMPYREAN). X-ray photoelectron spectroscopy (XPS) was used to demonstrate the presence of Ni^{2+} and Ni^{3+} ions in the sintered $La_{1.9}Sr_{0.1}Ni_{1-x}Mg_xO_4$ ceramics. XPS spectra were collected using a PHI5000 VersaProbe II (ULVAC-PHI, Japan). The PHI MultiPak XPS software and Gaussian−Lorentzian lines were used to obtain the Ni^{3+}/Ni^{2+} ratio.

For the electrical and dielectric measurements, the surfaces of the sintered ceramics were polished smoothly. The Au electrode was fabricated by sputtering onto polished surfaces using a Polaron SC500 sputter−coating unit. The dielectric properties of the $La_{1.9}Sr_{0.1}Ni_{1-x}Mg_xO$ ceramics as a function of frequency (10^2−10^6 Hz) and temperature (−70 to 150 °C) were investigated using a KEYSIGHT E4990A impedance analyzer. The ac conductivity (σ_{ac}) was calculated using the equation $\sigma_{ac} = \omega\varepsilon_o\varepsilon''$, where $\omega = 2\pi f$, ε_o is the permittivity of free space (8.854×10^{-12} F/m), and ε'' is the imaginary part of the complex dielectric permittivity, which was calculated by $\varepsilon'' = \varepsilon' \times \tan\delta$. At a low−frequency range, if σ_{ac} is dependent on frequency, σ_{ac} is approximately equal to the dc conductivity (σ_{dc}).

3. Results and discussion

The tetragonal structure of $La_{1.9}Sr_{0.1}Ni_{1-x}Mg_xO_4$ (JCPDS 32-1241) was confirmed using XRD, as shown in Fig. 1(a). These XRD patterns are similar to those reported in literature [24,29,33,36]. A single phase of LSNO was observed without any impurities. The combustion method was successfully used to produce $La_{1.9}Sr_{0.1}Ni_{1-x}Mg_xO_4$ ceramics. The lattice parameters (*a* and *c*) of all ceramic samples are shown in Fig. 1(b). Obviously, the cell parameters of the $La_{1.9}Sr_{0.1}Ni_{1-x}Mg_xO_4$ ceramics increased with increasing Mg^{2+} doping ions. This indicates that Mg^{2+} ions can be substituted into the lattice structure of the LSNO. The enlargement of the cell parameters results from the different ionic radii between the Ni^{2+} host ions ($r_4 = 0.55$ Å) and Mg^{2+} doping ions ($r_4 = 0.57$ Å) [46].

Fig. 2(a–d) shows the morphologies of all the sintered ceramics. A highly dense microstructure without porosity was achieved in all sintered ceramics. The relative density of all samples was ~98%. The mean grain size tended to decrease when Mg^{2+} increased, indicating that Mg^{2+} doping inhibited the grain growth rate of the $La_{1.9}Sr_{0.1}Ni_{1-x}Mg_xO_4$ ceramics [47]. The suppressed grain growth found in the $La_{1.9}Sr_{0.1}Ni_{1-x}Mg_xO_4$ ceramics because of Mg^{2+} is similar to that observed in Mg^{2+}-doped CCTO and $ACu_3Ti_4O_{12}$ ceramics [48,49]. Fig. 3(a–f) shows the microstructure analysis of the LSNO_Mg04 ceramic using the SEM−mapping technique. The Mg dopant and the major elements (La, Sr, Ni, and O) were well dispersed in the microstructure. No segregation of the Mg dopant at the grain boundaries or other regions was observed. This result supports the XRD result because Mg^{2+} ions can likely be substituted into the LSNO structure without the formation of a new phase, the second phase. It was also observed that some white points appeared on the SEM images (Fig. 2), whereas they cannot be detected by the SEM-mapping technique. These particles may be an impurity phase, which was segregated during the sintering process.

The AC conductivities (σ_{ac}) of the $La_{1.9}Sr_{0.1}Ni_{1-x}Mg_xO_4$ ceramics are shown in Fig. 4. The σ_{ac} in a low-frequency range is independent of the frequency, which is usually estimated to be the DC conductivity (σ_{dc}) [50]. The σ_{dc} value was estimated from the σ_{ac} at

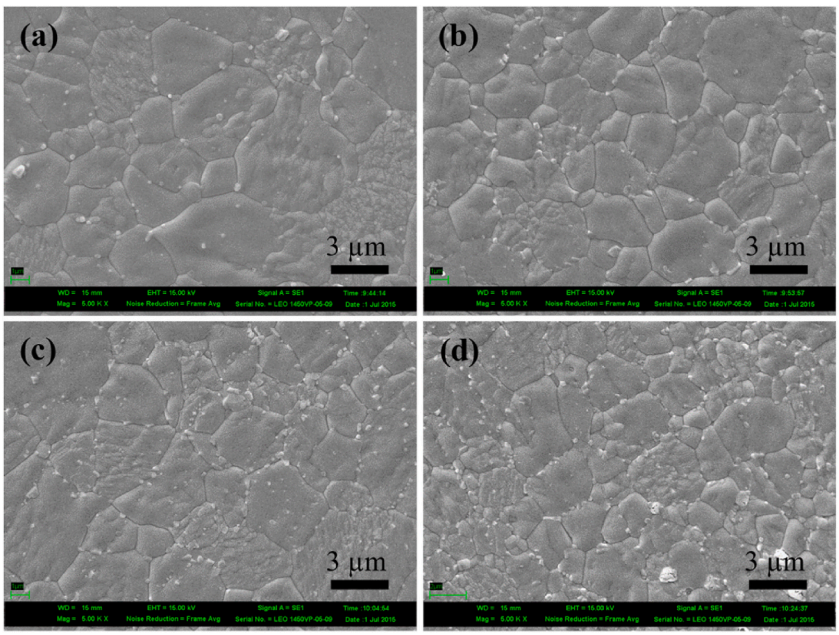

Fig. 2. SEM images of (a) LSNO, (b) LSNO_Mg03, (c) LSNO_Mg04, and (d) LSNO_Mg05 ceramics.

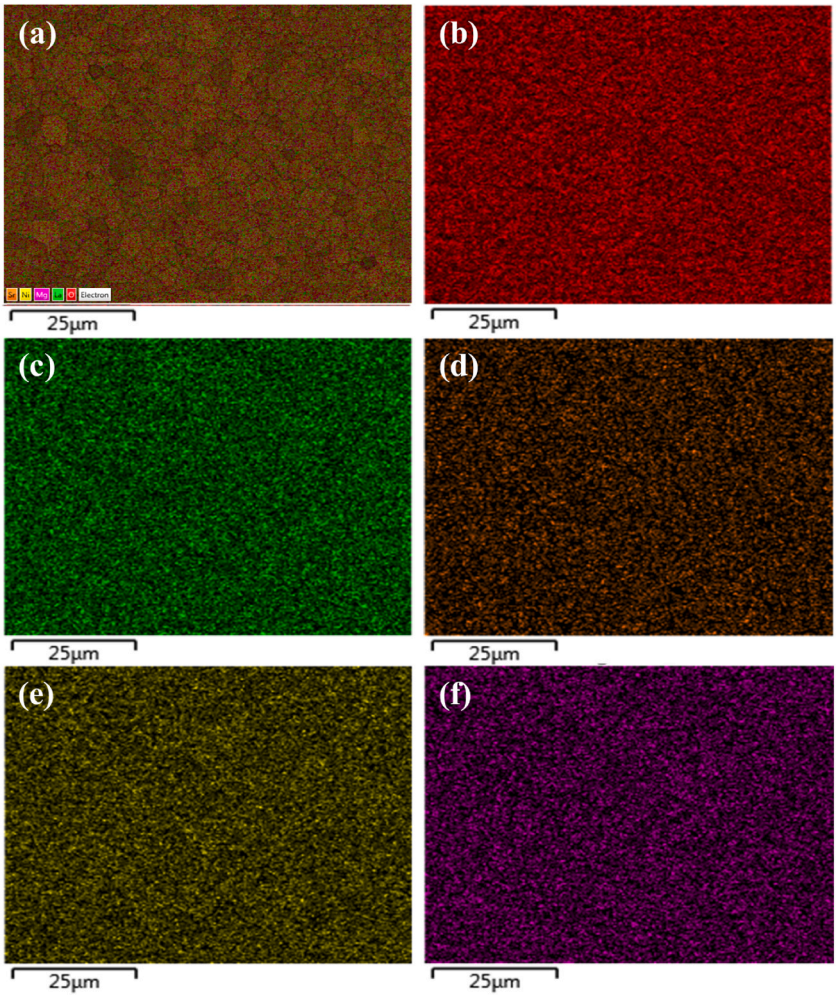

Fig. 3. SEM mapping images of LSNO_Mg04 ceramics; (a) all elements, (b) O, (c) La, (d) Sr, (e) Ni, and (f) Mg.

10^2 Hz. As clearly seen, σ the $_{dc}$ of the LSNO ceramics was significantly reduced by three orders of magnitude after doping with Mg^{2+} ions. The σ_{dc} values of the LSNO, LSNO_Mg03, LSNO_Mg04, and LSNO_Mg05 ceramics were 3.4×10^{-2}, 4.2×10^{-5}, 4.4×10^{-5}, and 6.1×10^{-5} S cm^{-1}, respectively. This indicates that doping LSNO with Mg^{2+} ions can enhance the total resistivity, which is significantly affected by the insulating grain boundaries. Therefore, doping LSNO with Mg^{2+} may reduce the long–range motion of free charge carriers (i.e., holes) and/or confining them inside an individual grain.

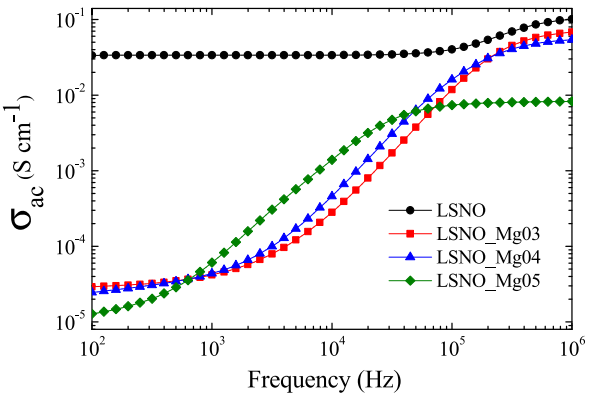

Fig. 4. Frequency dependence of AC conductivity (σac) for sintered ceramics at room temperature.

The GDR at different temperatures (−70 to 150 °C) at 100 Hz and 1 kHz for the sintered $La_{1.9}Sr_{0.1}Ni_{1-x}Mg_xO_4$ are displayed in Fig. 5(a and b), respectively. All the samples showed large ε′ values on the order of 10^5–10^6 over the measured temperature range. The ε′ of the $La_{1.9}Sr_{0.1}Ni_{1-x}Mg_xO_4$ ceramics changed slightly with the doping concentration. Furthermore, ε′ of all $La_{1.9}Sr_{0.1}Ni_{1-x}Mg_xO_4$ ceramics is slightly dependent on the temperature compared to that of the undoped ceramic. Surprisingly, tanδ of the LSNO ceramics was significantly reduced by at least two orders of magnitude after doping with Mg^{2+} ions. The ε′ values at 1 kHz and 20 °C of the LSNO_Mg03, LSNO_Mg04, and LSNO_Mg05 ceramics were 12.6×10^5, 6.96×10^5, 8.11×10^5, and 7.68×10^5, respectively, while the tanδ values were 11.76, 0.138, 0.099, and 0.200, respectively.

As clearly demonstrated in Fig. 6 and the inset, the resistance of the grain boundary (R_{gb}) of the LSNO ceramics was greatly increased by doping with Mg^{2+} ions, while the grain resistance (R_g) increased. It should be noted that the R_{gb} of the undoped LSNO was very low (~125 Ω cm), as shown in the inset of Fig. 6. The origin of the GDR in LSNO ceramics was described by the small polaron hopping and sample−electrode contact effect [25,38,39]. This was due to the very low R_{gb} value of LSNO. However, upon doping LSNO with Mg^{2+}, the R_{gb} values increased significantly. Therefore, the origin of the observed dielectric properties of the LSNO_Mg03, LSNO_Mg04, and LSNO_Mg05 ceramics should be primarily attributed to Maxwell–Wagner polarization. The significant reduction in tanδ in the $La_{1.9}Sr_{0.1}Ni_{1-x}Mg_xO_4$ ceramics can be explained by the extremely high R_{gb} value. It is worth noting that the dielectric properties of many giant dielectric oxides can be controlled by the electrical properties of the grain boundary such as CCTO [51–54] and related compounds [55]. Furthermore, the defect dipoles is one of the important key factors that can contribute the giant dielectric response and temperature stability of ε′, which has widely been reported in TiO_2 [17,19,20], $SrTiO_3$ [23], NiO [56], CCTO [57], and $BaTiO_3$-based materials [58,59].

The overall dielectric and electrical properties of the $La_{1.9}Sr_{0.1}Ni_{1-x}Mg_xO_4$ ceramics are shown in Fig. 7. The ε′ values at 1 kHz for the $La_{1.9}Sr_{0.1}Ni_{1-x}Mg_xO_4$ ceramics changed slightly as the concentration of Mg^{2+} increased. A correlation between tanδ (at 1 kHz) and R_{gb} was clearly observed. The extreme decrease in tanδ was attributed to the significant increase in R_{gb} [15,24,45]. The activation energies of all sintered ceramics were 0.109, 0.294, 0.383, and 0.404 eV for the LSNO, LSNO_Mg03, LSNO_Mg04, and LSNO_Mg05 ceramics, respectively. Thus, the increased R_{gb} value of the $La_{1.9}Sr_{0.1}Ni_{1-x}Mg_xO_4$ ceramics was due to the grain boundary properties caused by Mg^{2+} substitution.

Fig. 8 shows the XPS spectra of all sintered ceramics, confirming the existence of induced Ni^{3+} ions due to the partial replacement of La^{3+} by Sr^{2+} and oxygen ion enrichment. However, the concentration of Ni^{3+} ions was reduced in the LSNO_Mg03, LSNO_Mg04, and LSNO_Mg05 ceramics compared to that in the undoped LSNO ceramic. This may be due to the substitution of Mg^{2+} into the Ni^{3+} sites and/or the reduced enrichment of oxygen ions in the structure. The GDR cannot be described by small polaron hopping only because the value of ε′ is not correlated with the ratio of Ni^{3+}/Ni^{2+} ions. Another important factor is interfacial polarization at the grain boundaries. This can also cause an increase in the dielectric response of LSNO ceramics.

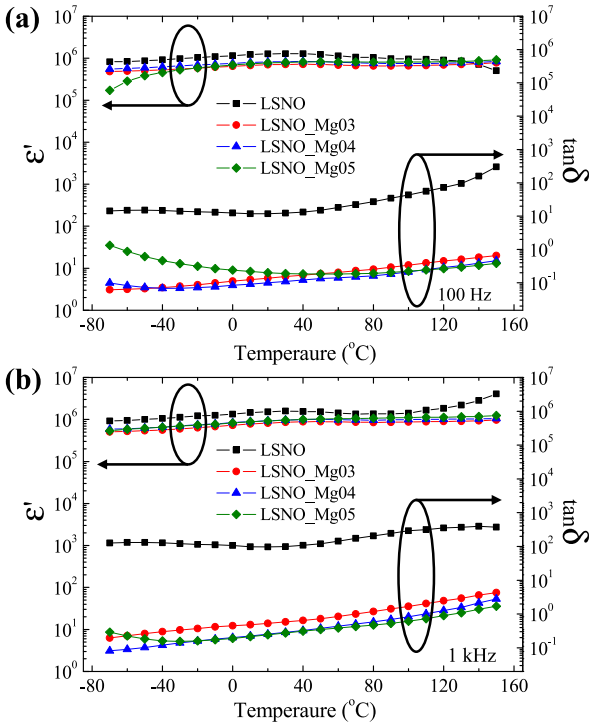

Fig. 5. Temperature dependence of dielectric permittivity (ε′) and loss tangent (tanδ) for ceramics sintered at (a) 100 Hz and (b) 1 kHz.

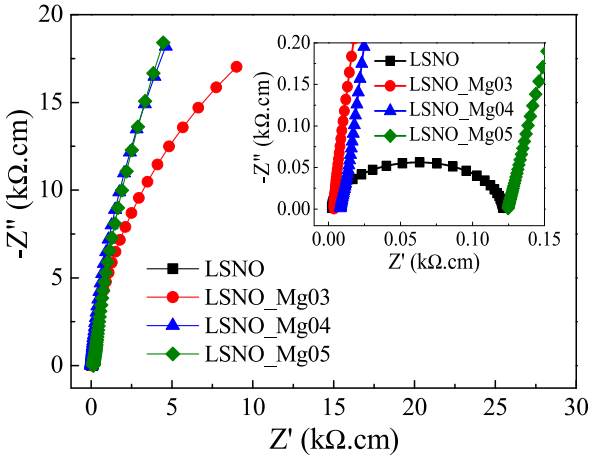

Fig. 6. Impedance complex plane plots of the ceramics sintered at 20 °C; the inset shows an expanded view of the high-frequency data close to the origin.

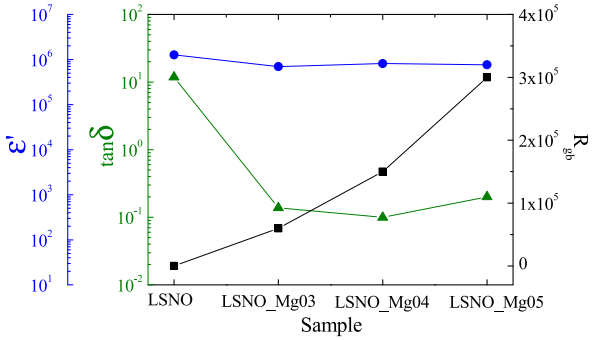

Fig. 7. ε′, tanδ, and Rgb values of ceramics sintered at 20 °C.

4. Conclusions

In conclusion, an extremely reduced loss tangent with ultrahigh ε′ can be successfully obtained in LSNO ceramics by doping with Mg^{2+} ions. A single phase of LSNO was detected in all the sintered ceramics, while the lattice parameters increased with increasing doping concentration, indicating that Mg^{2+} ions can enter the Ni^{2+} sites. A highly dense microstructure is achieved. Microstructural analysis revealed that Mg^{2+} ions disperse well in the microstructure of LSNO ceramics. Interestingly, ultra–high ε′ of approximately 8.11×10^5 at 1 kHz is achieved in the $La_{1.9}Sr_{0.1}Ni_{0.6}Mg_{0.4}O_4$ ceramic, while the tanδ is significantly reduced by two orders of magnitude compared to the undoped LSNO ceramic. The DC conductivity significantly decreased by three orders of magnitude. The GDRs are described by Maxwell–Wagner polarization and small polaron hopping mechanisms. Thus, the significant reduction in the tanδ can be attributed to the significantly enhanced R_{gb}.

Author contribution statement

Keerati Meeporn: Conceived and designed the experiments; Performed the experiments; Analyzed and interpreted the data; Wrote the paper.

Narong Chanlek, Pornjuk Srepusharawoot: Performed the experiments; Analyzed and interpreted the data.

Prasit Thongbai: Conceived and designed the experiments; Analyzed and interpreted the data; Contributed reagents, materials, analysis tools or data; Wrote the paper.

Funding statement

This work was supported by National Research Council of Thailand (NRCT) (N41A640084), Thailand Research Fund under the Royal Golden Jubilee (PHD/0191/2556) and by Research and Graduate Studies, Khon Kaen University.

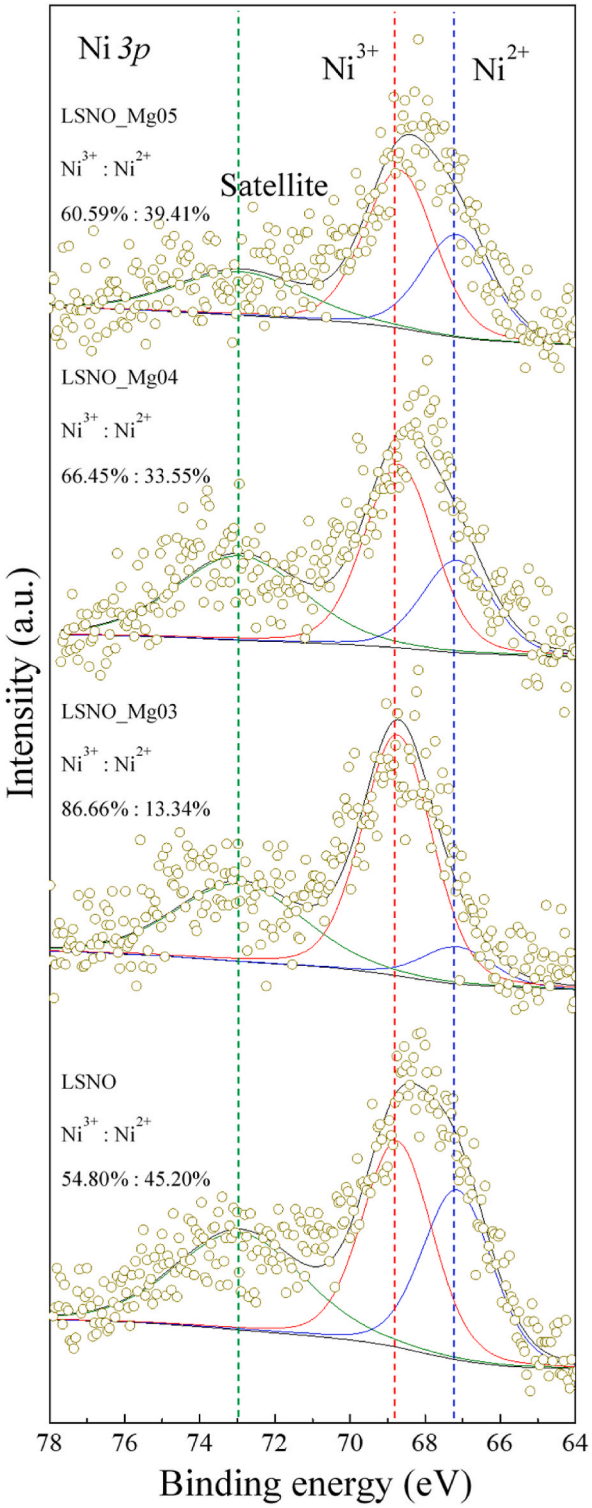

Fig. 8. XPS spectra of all sintered $La_{1.9}Sr_{0.1}Ni_{1-x}Mg_xO_4$ ceramics.

Data availability statement

Data will be made available on request.

Declaration of interest's statement

The authors declare that they have no known competing financial interests or personal relationships that could have appeared to influence the work reported in this paper.

References

[1] H.M. Kotb, M.M. Ahmad, A. Alshoaibi, K. Yamada, Dielectric response and structural analysis of (A^{3+}, Nb^{5+}) cosubstituted $CaCu_3Ti_4O_{12}$ ceramics (A: Al and Bi), Materials 13 (2020) 5822.

[2] R. Xue, Y. Chen, T. Li, D. Liu, S. Chen, H. Chen, M. Cui, Effects of Lu^{3+} doping on microstructures and electrical properties of $CaCu_3Ti_4O_{12}$ ceramics, J. Supercond. Nov. Magnetism 34 (2021) 3297–3309.

[3] M. Chinnathambi, A. Sakthisabarimoorthi, M. Jose, R. Robert, Study of the Electrical and Dielectric behaviour of selenium doped CCTO ceramics prepared by a facile sol-gel route, Mater. Chem. Phys. 272 (2021), 124970.

[4] Y. Li, W. Li, G. Du, N. Chen, Low temperature preparation of $CaCu_3Ti_4O_{12}$ ceramics with high permittivity and low dielectric loss, Ceram. Int. 43 (2017) 9178–9183.

[5] Z. Peng, J. Wang, X. Lei, J. Zhu, S. Xu, P. Liang, L. Wei, D. Wu, J. Wang, X. Chao, Z. Yang, Colossal dielectric response in $CdAl_xCu_{3-x}Ti_4O_{12}$ perovskite ceramics, Mater. Chem. Phys. 258 (2021), 123940.

[6] Z. Peng, X. Zhou, J. Wang, J. Zhu, P. Liang, X. Chao, Z. Yang, Origin of colossal permittivity and low dielectric loss in $Na_{1/3}Cd_{1/3}Y_{1/3}Cu_3Ti_4O_{12}$ ceramics, Ceram. Int. 46 (2020) 11154–11159.

[7] G. Du, F. Wei, W. Li, N. Chen, Co-doping effects of A-site Y^{3+} and B-site Al^{3+} on the microstructures and dielectric properties of $CaCu_3Ti_4O_{12}$ ceramics, J. Eur. Ceram. Soc. 37 (2017) 4653–4659.

[8] Z. Peng, J. Wang, X. Zhou, J. Zhu, X. Lei, P. Liang, X. Chao, Z. Yang, Grain engineering inducing high energy storage in $CdCu_3Ti_4O_{12}$ ceramics, Ceram. Int. 46 (2020) 14425–14430.

[9] G. Miao, M. Yin, P. Li, J. Hao, W. Li, J. Du, G. Li, C. Wang, P. Fu, Effect of Cr addition on the structure and electrical properties of $CaCu_3Ti_4O_{12}$ NTC thermistor, J. Alloys Compd. 884 (2021), 161066.

[10] P. Mao, J. Wang, P. Xiao, L. Zhang, F. Kang, H. Gong, Colossal dielectric response and relaxation behavior in novel system of Zr^{4+} and Nb^{5+} co-substituted $CaCu_3Ti_4O_{12}$ ceramics, Ceram. Int. 47 (2021) 111–120.

[11] T. Prakash, B.S. Murty, A.R. Kaskhedikar, P.D. Peshwe, Crystallite size effect on voltage tunable giant dielectric permittivity of nanocrystalline CuO, Electron. Mater. Lett. 9 (2013) 59–62.

[12] S. Tangwancharoen, P. Thongbai, T. Yamwong, S. Maensiri, Dielectric and electrical properties of giant dielectric (Li, Al)-doped NiO ceramics, Mater. Chem. Phys. 115 (2009) 585–589.

[13] Y. Liu, W. Wang, J. Huang, C. Zhu, C. Wang, Y. Cao, High dielectric permittivity of Li and Sc co-doped NiO ceramics, J. Mater. Sci. Mater. Electron. 25 (2014) 1298–1302.

[14] Y. Huang, D. Shi, L. Liu, G. Li, S. Zheng, L. Fang, High-temperature impedance spectroscopy of $BaFe_{0.5}Nb_{0.5}O_3$ ceramics doped with $Bi_{0.5}Na_{0.5}TiO_3$, Appl. Phys. A 114 (2014) 891–896.

[15] W. Tuichai, S. Danwittayakul, J. Manyam, N. Chanlek, M. Takesada, P. Thongbai, Giant dielectric properties of Ga^{3+}-Nb^{5+}Co-doped TiO_2 ceramics driven by the internal barrier layer capacitor effect, Materialia 18 (2021), 101175.

[16] A.M. Youssef, S.M. Yakout, Colossal permittivity, electrical conductivity and ferromagnetic properties of pure TiO_2: mono and binary doping, Materialia 21 (2022), 101277.

[17] P. Liang, J. Zhu, D. Wu, H. Peng, X. Chao, Z. Yang, Good dielectric performance and broadband dielectric polarization in Ag, Nb co-doped TiO_2, J. Am. Ceram. Soc. 104 (2021) 2702–2710.

[18] X. Zhou, P. Liang, J. Zhu, Z. Peng, X. Chao, Z. Yang, Enhanced dielectric performance of $(Ag_{1/4}Nb_{3/4})_{0.01}Ti_{0.99}O_2$ ceramic prepared by a wet-chemistry method, Ceram. Int. 46 (2020) 11921–11925.

[19] P. Peng, C. Chen, B. Cui, J. Li, D. Xu, B. Tang, Influence of the electric field on flash-sintered (Zr + Ta) co-doped TiO_2 colossal permittivity ceramics, Ceram. Int. 48 (2022) 6016–6023.

[20] Z. Wang, P. Peng, L. Zhang, N. Wang, B. Tang, B. Cui, J. Liu, D. Xu, Effect of electric field on the microstructure and electrical properties of (In + Ta) co-doped TiO_2 colossal dielectric ceramics, J. Mater. Sci. Mater. Electron. 33 (2022) 6283–6293.

[21] Y. Chao, W. Xianhua, H. Jianhua, Colossal permittivity in TiO_2 co-doped by donor Nb and isovalent Zr, J. Am. Ceram. Soc. 101 (2018) 307–315.

[22] J. Li, Y. Zeng, Y. Fang, N. Chen, G. Du, A. Zhang, Synthesis of (La + Nb) co-doped TiO_2 rutile nanoparticles and dielectric properties of their derived ceramics composed of submicron-sized grains, Ceram. Int. 47 (2021) 8859–8867.

[23] Y. Chen, Y. Zeng, W. Cao, N. Chen, G. Du, Colossal permittivity and low dielectric loss in (Li, Nb) co-doped $SrTiO_3$ ceramics with high frequency and temperature stability, Ceram. Int. 48 (2022) 36393–36400.

[24] K. Meeporn, N. Chanlek, P. Thongbai, Effects of DC bias on non-ohmic sample-electrode contact and grain boundary responses in giant-permittivity $La_{1.7}Sr_{0.3}Ni_{1-x}Mg_xO_4$ ceramics, RSC Adv. 6 (2016) 91377–91385.

[25] S. Krohns, P. Lunkenheimer, C. Kant, A.V. Pronin, H.B. Brom, A.A. Nugroho, M. Diantoro, A. Loidl, Colossal dielectric constant up to gigahertz at room temperature, Appl. Phys. Lett. 94 (2009), 122903.

[26] X.Q. Liu, Y.J. Wu, X.M. Chen, H.Y. Zhu, Temperature-stable giant dielectric response in orthorhombic samarium strontium nickelate ceramics, J. Appl. Phys. 105 (2009), 054104.

[27] K. Meeporn, S. Maensiri, P. Thongbai, Abnormally enhanced dielectric permittivity in poly(vinylidene fluoride)/nanosized-$La_2NiO_{4-\delta}$ films, Appl. Surf. Sci. 380 (2016) 67–72.

[28] X.Q. Liu, G. Liu, P.P. Ma, G.J. Li, J.W. Wu, X.M. Chen, Giant dielectric response with reduced loss in ceramics with nominal composition of $La_{1.5}Sr_{0.5}NiO_4$-SiO_2, J. Electroceram.37 (2016) 73–78.

[29] K. Meeporn, T. Yamwong, P. Thongbai, $La_{1.7}Sr_{0.3}NiO_4$ nanocrystalline powders prepared by a combustion method using urea as fuel: preparation, characterization, and their bulk colossal dielectric constants, Jpn. J. Appl. Phys. 53 (2014), 06JF01.

[30] P. Thongbai, T. Yamwong, S. Maensiri, Microstructure and modified giant dielectric response in Ga-doped $La_{1.5}Sr_{0.5}NiO_4$ ceramics, Mater. Lett. 82 (2012) 244–247.

[31] Y. Wang, W. Jie, C. Yang, X. Wei, J. Hao, Colossal permittivity materials as superior dielectrics for diverse applications, Adv. Funct. Mater. 29 (2019), 1808118.

[32] S. Krohns, P. Lunkenheimer, S. Meissner, A. Reller, B. Gleich, A. Rathgeber, T. Gaugler, H.U. Buhl, D.C. Sinclair, A. Loidl, The route to resource-efficient novel materials, Nat. Mater. 10 (2011) 899–901.

[33] X.Q. Liu, Y.J. Wu, X.M. Chen, Giant dielectric response and polaronic hopping in charge-ordered ceramics, Solid State Commun. 150 (2010) 1794–1797.

[34] G. Liu, T.T. Chen, J. Wang, X.Q. Liu, X.M. Chen, Effect of excess oxygen on crystal structures and dielectric responses of $Nd_2NiO_{4+\delta}$ ceramics, J. Alloys Compd. 579 (2013) 502–506.

[35] B. Wen Jia, X. Qiang Liu, X. Ming Chen, Structure, magnetic and dielectric properties in Mn-substituted $Sm_{1.5}Sr_{0.5}NiO_4$ ceramics, J. Appl. Phys. 110 (2011), 064110.

[36] X.Q. Liu, S.Y. Wu, X.M. Chen, Enhanced giant dielectric response in Al-substituted $La_{1.75}Sr_{0.25}NiO_4$ ceramics, J. Alloys Compd. 507 (2010) 230–235.

[37] X.Q. Liu, B.W. Jia, W.Z. Yang, J.P. Cheng, X.M. Chen, Dielectric relaxation and polaronic hopping in Al-substituted $Sm_{1.5}Sr_{0.5}NiO_4$ ceramics, J. Phys. D Appl. Phys. 43 (2010), 495402.

[38] X.Q. Liu, S.Y. Wu, X.M. Chen, H.Y. Zhu, Giant dielectric response in two-dimensional charge-ordered nickelate ceramics, J. Appl. Phys. 104 (2008), 054114.

[39] M. Li, D.C. Sinclair, The extrinsic origins of high permittivity and its temperature and frequency dependence in $Y_{0.5}Ca_{0.5}MnO_3$ and $La_{1.5}Sr_{0.5}NiO_4$ ceramics, J. Appl. Phys. 111 (2012), 054106.

[40] B.W. Jia, W.Z. Yang, X.Q. Liu, X.M. Chen, Giant dielectric response in $(Sm_{1-x}Nd_x)_{1.5}Sr_{0.5}NiO_4$ ceramics: the intrinsic and extrinsic effects, J. Appl. Phys. 112 (2012), 024104.

[41] P. Lunkenheimer, S. Krohns, S. Riegg, S.G. Ebbinghaus, A. Reller, A. Loidl, Colossal dielectric constants in transition-metal oxides, Eur. Phys. J. Spec. Top. 180 (2010) 61–89.

[42] M. Li, D.C. Sinclair, A.R. West, Extrinsic origins of the apparent relaxorlike behavior in $CaCu_3Ti_4O_{12}$ ceramics at high temperatures: a cautionary tale, J. Appl. Phys. 109 (2011), 084106.

[43] P. Siriya, A. Pengpad, P. Srepusharawoot, N. Chanlek, P. Thongbai, Improved microstructure and significantly enhanced dielectric properties of $Al^{3+}/Cr^{3+}/Ta^{5+}$ triple-doped TiO_2 ceramics by Re-balancing charge compensation, RSC Adv. 12 (2022) 4946–4954.

[44] P. Siriya, N. Chanlek, P. Srepusharawoot, V. Harnchana, P. Thongbai, Triple-doping of $(Ga_{1/2}Nb_{1/2})_xTi_{1-x}O_2$ ceramics with Al^{3+} for enhanced giant dielectric response with simultaneous decrease in dielectric loss, J. Eur. Ceram. Soc. 42 (2022) 2798–2803.

[45] Z. Peng, D. Wu, P. Liang, X. Zhou, J. Wang, J. Zhu, X. Chao, Z. Yang, Grain boundary engineering that induces ultrahigh permittivity and decreased dielectric loss in $CdCu_3Ti_4O_{12}$ ceramics, J. Am. Ceram. Soc. 103 (2020) 1230–1240.

[46] R.D. Shannon, Revised effective ionic radii and systematic Studies of interatomie distances in halides and chaleogenides, Acta Crystallogr. A32 (1976) 751–767.

[47] M.N. Rahaman, Ceramic Processing and Sintering, second ed., M. Dekker, New York, 2003.

[48] J. Boonlakhorn, P. Kidkhunthod, P. Thongbai, A novel approach to achieve high dielectric permittivity and low loss tangent in $CaCu_3Ti_4O_{12}$ ceramics by co-doping with Sm^{3+} and Mg^{2+} ions, J. Eur. Ceram. Soc. 35 (2015) 3521–3528.

[49] Z. Peng, X. Wang, S. Xu, F. Zhang, J. Wang, J. Wang, D. Wu, P. Liang, L. Wei, X. Chao, Z. Yang, Improved grain boundary resistance inducing decreased dielectric loss and colossal permittivity in $Y_{2/3}Cu_3Ti_4O_{12}$ ceramics, Mater. Chem. Phys. (2022), 125874.

[50] C.L. Song, Y.J. Wu, X.Q. Liu, X.M. Chen, Dielectric properties of $La_{1.75}Ba_{0.25}NiO_4$ ceramics prepared by spark plasma sintering, J. Alloys Compd. 490 (2010) 605–608.

[51] L. Liu, L. Fang, Y. Huang, Y. Li, D. Shi, S. Zheng, S. Wu, C. Hu, Dielectric and nonlinear current–voltage characteristics of rare–earth doped $CaCu_3Ti_4O_{12}$ ceramics, J. Appl. Phys. 110 (2011), 094101.

[52] Y. Huang, L. Liu, D. Shi, S. Wu, S. Zheng, L. Fang, C. Hu, B. Elouadi, Giant dielectric permittivity and non-linear electrical behavior in $CaCu_3Ti_4O_{12}$ varistors from the molten-salt synthesized powder, Ceram. Int. 39 (2013) 6063–6068.

[53] Y. Huang, D. Shi, Y. Li, G. Li, Q. Wang, L. Liu, L. Fang, Effect of holding time on the dielectric properties and non-ohmic behavior of $CaCu_3Ti_4O_{12}$ capacitor-varistors, J. Mater. Sci. Mater. Electron. 24 (2013) 1994–1999.

[54] J. Deng, X. Sun, S. Liu, L. Liu, T. Yan, L. Fang, B. Elouadi, Influence of interface point defect on the dielectric properties of Y doped $CaCu_3Ti_4O_{12}$ ceramics, J. Adv. Dielectr. 6 (2016), 1650009.

[55] G. Li, Z. Chen, X. Sun, L. Liu, L. Fang, B. Elouadi, Electrical properties of $AC_3B_4O_{12}$-type perovskite ceramics with different cation vacancies, Mater. Res. Bull. 65 (2015) 260–265.

[56] Y. Li, L. Fang, L. Liu, Y. Huang, C. Hu, Giant dielectric response and charge compensation of Li- and Co-doped NiO ceramics, Mater. Sci. Eng. B 177 (2012) 673–677.

[57] F. Han, S. Ren, J. Deng, T. Yan, X. Ma, B. Peng, L. Liu, Dielectric response mechanism and suppressing high-frequency dielectric loss in Y_2O_3 grafted $CaCu_3Ti_4O_{12}$ ceramics, J. Mater. Sci. Mater. Electron. 28 (2017) 17378–17387.

[58] Y. Meng, K. Liu, X. Zhang, X. Qiang, X. Lei, J. Chen, C. Li, Z. Yang, L. Liu, Compositional modulation and annealing treatment in $BaTiO_3$ to simultaneously achieve colossal permittivity, low dielectric loss, and high thermal stability, Ceram. Int. 47 (2021) 33912–33916.

[59] Y. Meng, K. Liu, X. Zhang, X. Lei, J. Chen, Z. Yang, B. Peng, C. Long, L. Liu, C. Li, Defect engineering in rare-earth-doped $BaTiO_3$ ceramics: route to high-temperature stability of colossal permittivity, J. Am. Ceram. Soc. 105 (2022) 5725–5737.